Infrared and broadband dielectric spectroscopy of PZN-PMN-PSN relaxor ferroelectrics: Origin of two-component relaxation

J. Macutkevic,[1,*] S. Kamba,[2] J. Banys,[1] A. Brilingas,[1] A. Pashkin,[2,4] J. Petzelt,[2] K. Bormanis,[3] and A. Sternberg[3]
[1]*Faculty of Physics, Vilnius University, Sauletekio 9, Vilnius LT-10222, Lithuania*
[2]*Institute of Physics, ASCR, Na Slovance 2, 18221 Prague 8, Czech Republic*
[3]*Institute of Solid State Physics, University of Latvia, 8 Kengaraga, 1063 Riga, Latvia*
[4]*Physikalisches Institut, Universität Stuttgart, Pfaffenwaldring 57, 70550 Stuttgart, Germany*
(Received 4 April 2006; revised manuscript received 12 June 2006; published 12 September 2006)

Dielectric spectra of several solid solutions of $PbMg_{1/3}Nb_{2/3}O_3$-$PbSc_{1/2}Nb_{1/2}O_3$-$PbZn_{1/3}Nb_{2/3}O_3$ (PMN-PSN-PZN) relaxor ferroelectrics were investigated in a broad frequency range from 20 Hz up to 100 THz by a combination of dielectric spectroscopy (20 Hz–53 GHz), time-domain terahertz spectroscopy (0.1–0.9 THz), and infrared reflectivity (20–3000 cm^{-1}, 0.6–90 THz). The very strong and broad dielectric relaxation observed below phonon frequencies was analyzed in terms of the distribution of relaxation times, using the Tichonov regularization method. This revealed slowing down of the longest and mean relaxation times obeying the Vogel-Fulcher law. The relaxation splits into two components near T_m and the origin of both components is discussed. The formation of polar clusters below the Burns temperature (700–800 K) is manifested by the appearance of dielectric relaxation in the terahertz range and by splitting of the polar modes in the infrared spectra. On heating from low temperatures, the A_1 component of the strongly split TO_1 mode softens toward the Burns temperature, but the softening ceases near 400 K, which could be a signature of a polar cluster percolation temperature.

DOI: 10.1103/PhysRevB.74.104106 PACS number(s): 77.22.−d, 78.30.−j, 63.20.−e, 71.55.Jv

I. INTRODUCTION

Relaxor ferroelectrics (RFEs) have attracted considerable attention in recent years due to their unusual physical behavior and excellent dielectric and electromechanical properties. Many physical models have been proposed to explain the unusual behavior of the RFEs, for example, the diffuse phase transition model, the superparaelectric model, the dipolar glass model, the order-disorder model, the random field model, and the spherical random bond–random field model;[1,2] however, quantitative understanding of the complex dielectric behavior in RFEs is still not satisfactory.

$PbMg_{1/3}Nb_{2/3}O_3$ (PMN), $PbSc_{1/2}Nb_{1/2}O_3$ (PSN), and $PbZn_{1/3}Nb_{2/3}O_3$ (PZN) are typical RFE crystals with perovskite structure. All these compounds exhibit a large, diffuse, and frequency-dependent maximum in the temperature plot of the complex permittivity. No breaking of cubic symmetry was observed in PMN at any temperature without a bias electric field;[3] however, for PSN and PZN a ferroelectric phase transition from the cubic to the rhombohedral phase was reported near 360 (Refs. 4 and 5) and 410 K,[6,7] respectively. Nevertheless, there are indications from various experiments (the temperature dependence of the index of refraction,[8] x-ray diffraction, quasielastic neutron at the Burns temperature T_d scattering,[9,10] etc.) that the cubic crystal structure in RFEs is locally broken already about 300 K above the temperature of the permittivity maximum T_m. The regions in which the cubic structure is broken are called polar nanoclusters or nanoregions. Concerning their symmetry, many authors assume that the nanoregions have the same symmetry as the low-temperature ferroelectric phase, i.e., rhombohedral, although it was not confirmed experimentally. An x-ray diffraction study[11] of PMN revealed only spherically symmetric displacements of lead ions from the perovskite *A* sites below T_d, which would mean nonpolar symmetry. This is probably an unrealistic result, but the fact of spherically symmetrical displacement of Pb ions was successfully exploited in the spherical random bond–random field model.[1]

Nowadays, it is generally accepted that the complex dielectric properties are connected with the chemical disorder of ions with different valency at the *B* perovskite sites. For example, *B* sites of PSN contain 50% of Sc^{3+} and 50% of Nb^{5+} ions and, if these ions are statistically disordered, PSN exhibits relaxor ferroelectric behavior above the ferroelectric phase transition (380 K).[4] If the ions are 1:1 chemically ordered, which can be achieved by proper annealing, PSN shows only a sharp ferroelectric transition and its temperature shifts to 340 K.[4] The PMN and PZN is more complicated. Mg^{2+} and Nb^{5+} or Zn^{2+} and Nb^{5+} have the ratio 1:2 at the *B* sites and cannot be long-range ordered by any heat treatment. Only a short-range 1:1 order on a length scale of 20–50 Å is possible in the *B* sites. One site is occupied by Nb^{5+} and the other one by a random mixture of 1/3 Nb^{5+} and 2/3 Mg^{2+} (in PMN) or of 1/3 Nb^{5+} and 2/3 Zn^{2+} (in PZN).[12] Although PZN and PMN RFEs are chemically and structurally similar, only the former exhibits a ferroelectric phase transition. On the other hand, in the related compound $PbMg_{1/3}Ta_{2/3}O_3$ (PMT), the *B* ions can be ordered by a proper annealing,[13] but it has insignificant influence on the dielectric properties—the RFE properties do not disappear in ordered PMT, in contrast to ordered PST or PSN.

Recent first-principle studies of PSN have shown that polar nanoregions appear more likely in chemically ordered nanoregions;[14] however, this statement was not yet confirmed experimentally in any RFE. Nevertheless, it is worth noting that, although the characteristic length scale for polar nanoregions is the same as for chemical short-range order at

B sites,[14] the polarization of the nanoregions is predominantly caused by dynamical disorder of Pb ions at the *A* perovskite sites.[10,11] Hopping of the disordered Pb ions among several closely spaced equivalent sites is mainly responsible for the huge permittivity in Pb-based perovskites. Chemical disorder at the *B* sites produces random fields, which cause smearing (i.e., distribution) of energy barriers for hopping of Pb ions. This causes broadening of the strong dielectric relaxation below the polar phonon frequencies, which at low temperatures becomes anomalously broad (from subhertz up to the terahertz range). Broadband dielectric spectroscopy is needed for investigation of such wide dielectric relaxations and since the microwave (MW) and terahertz techniques are rather difficult, only a few RFE systems (PMN,[15,16] PST,[17–19] and PLZT[20,21]) have so far been investigated in the MW and THz range simultaneously.

Dielectric and piezoelectric studies of solid solutions of RFEs like PMN and PSN with normal ferroelectric $PbTiO_3$ revealed giant piezoelectricity for compositions near the morphotropic phase boundary[22] (one order of magnitude larger than in the best classical ferroelectrics like $PbZr_{1-x}Ti_xO_3$). The paper of Park and Shrout[22] turned the attention of many physicists to the study of solid solutions of RFEs with ferroelectrics. Close to the morphotrophic phase boundary between the tetragonal and rhombohedral phases, a monoclinic phase was revealed at lower temperatures[23] and it was proposed that the easy rotation of polarization in the monoclinic phase is responsible for the giant piezoelectric coefficient in these systems.[24]

Solid solutions of two relaxor ferroelectrics were also investigated, although it is intuitively expected that such solid solutions will exhibit again relaxor behavior. The best investigated system is the PMN-PSN solid solution.[25–31] Relaxor behavior was observed in both ordered and disordered forms of $(1-x)$PMN-(x)PSN for $x \lesssim 0.6$.[28,29] At higher levels of substitution, the dielectric response was dependent on the degree of order: disordered samples were relaxors and ordered samples exhibited normal ferroelectric behavior. A NMR study of PMN-PSN revealed that the spherical model of Pb displacements is unable to yield the observed distribution of the shortest Pb-O bond length.[30]

Ternary solid solutions of PSN-PZN-PMN relaxor ferroelectrics were first synthesized and investigated by Dambekalne *et al.*[32] The system was very easily soluble and the dielectric data showed high values of permittivity (7000–30 000) with a diffuse peak typical for RFEs. Preliminary dielectric spectra of 0.2PMN-0.4PSN-0.4PZN and 0.4PSN-0.3PMN-0.3PZN ceramics were published by some of us.[33,34] It was shown that the dielectric relaxation is so broad in these systems that it can be described by the Cole-Cole model[35] only above room temperature. At lower temperatures, this model, as well as the Davidson-Cole, Williams-Watts, Havriliak-Negami,[36] Joncher, Kohlrausch-Williams-Watt and Curie–von Schweidler models[37] are not longer suitable for ferroelectric relaxors. We will show in this paper that the distribution of Debye relaxation times can be calculated from the experimental dielectric spectra. Broadband dielectric spectra (not only from the kilohertz and megahertz but also from the microwave and terahertz range) are needed for such a computation. Therefore we have performed a detailed dielectric study of five different ceramics (see Table I) in the range 20 Hz–150 THz including the experimentally difficult MW and THz spectral range. The temperature dependence of the distribution of relaxation times will be discussed in detail. For dynamics study of polar clusters near the Burns temperature we performed THz experiments up to 900 K.

TABLE I. Parameters of the Vogel-Fulcher fit of the mean relaxation time τ_{CC} for PZN-PMN-PSN ceramics.

Compound	τ_0 (s)	T_0 (K)	E/K (K)
0.4PZN-0.3PMN-0.3PSN	1×10^{-14}	200	1297.4
0.4PSN-0.3PMN-0.3PZN	1×10^{-14}	231.5	1077
0.2PSN-0.4PMN-0.4PZN	1×10^{-14}	250	829
0.4PMN-0.3PSN-0.3PZN	1.5×10^{-14}	210	1150
0.2PMN-0.4PSN-0.4PZN	6.27×10^{-14}	241	892

II. EXPERIMENT

The ternary PSN-PZN-PMN solid solution was synthesized by solid state reaction from high-grade oxides PbO_3, Nb_2O_5, MgO, ZnO, and Sc_2O_3. The primary ingredients were homogenized and milled in an agate ball mill for 8 h in ethanol and dried at 250 °C for 24 h. The dried mixture was fired in platinum crucibles. To obtain a sufficient homogeneous mixture of perovskite structure, the synthesis was repeated three times: first at 800 °C, the second at 900 °C, and the third at 1000 °C, for 2 h each. After each synthesis the mixture was milled in agate ball mill in ethanol, dried at 250 °C for 24 h, and the phase composition was analyzed by x-ray diffraction. Detailed processing and sintering conditions are given in Ref. 32.

The low-frequency dielectric response in the range of 20 Hz–1 MHz was measured using a HP 4284 LCR meter with an ac field of 1 V/mm on a sintered 5-mm-diameter cylinder. Dielectric measurements in the high-frequency range of 10 MHz–1.25 GHz were performed using a computer-controlled high frequency (HF) dielectric spectrometer. The dielectric parameters were calculated taking into account the electromagnetic field distribution in the sample.[38] In the frequency ranges 8–11 and 26–53 GHz an automatic waveguide dielectric spectrometer was used.[38] In these frequency ranges cylindrical-shaped samples with diameter ≈0.05 mm and length 6–11 mm were used. For all measurements silver paste was used for contacts.

Measurements at THz frequencies from 3 to 30 cm^{-1} (90–900 GHz) were performed in the transmission mode using a time-domain THz spectrometer based on an amplified femtosecond laser system. The technique itself works up to 80 cm^{-1}, but the samples were opaque above 30 cm^{-1}. Two ZnTe crystal plates were used to generate (by optic rectification) and detect (by electro-optic sampling) the THz pulses. Polished plane-parallel 40-μm-thick disks with a diameter of 6 mm were prepared. An Optistat CF cryostat with thin Mylar windows was used for measurements down to 20 K.

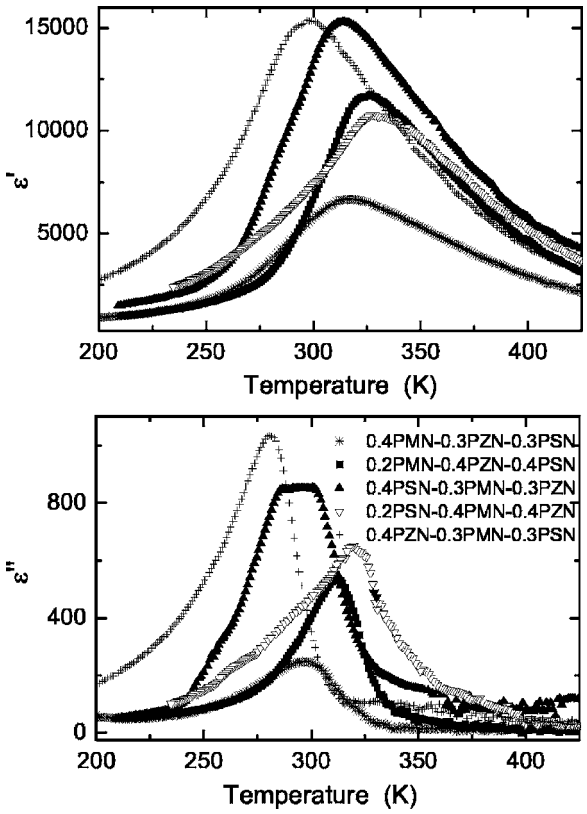

FIG. 1. Temperature dependence of the complex dielectric permittivity of various PZN-PMN-PSN ceramics measured at 1 kHz.

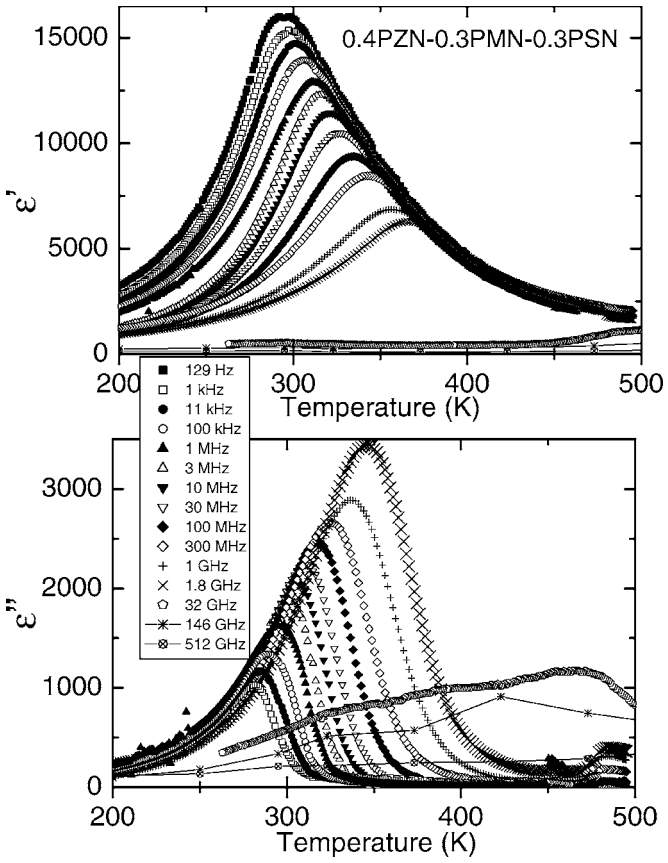

FIG. 2. Temperature dependence of the complex dielectric permittivity of 0.4PZN-0.3PMN-0.3PSN ceramics at several frequencies.

For sample heating, we used an adapted commercial high-temperature cell (SPECAC P/N 5850) with 1-mm-thick sapphire windows.

Infrared (IR) reflectivity spectra were obtained using a Fourier transform IR spectrometer Bruker IFS 113v in the frequency range of 20–3300 cm^{-1} (0.6–100 THz) above room temperature; at lower temperature the reduced spectral range up to 650 cm^{-1} was investigated because this is the transparency region of the polyethylene windows in the cryostat (Oxford Instruments). Pyroelectric deuterated triglycine sulfate detectors were used for the room- and higher-temperature measurements, while a more sensitive helium-cooled (1.5 K) Si bolometer was used for low-temperature measurements. A home-made furnace was used for high-temperature experiments up to 523 K. Polished disk-shaped samples with a diameter of 6 mm and thickness of ~2 mm were investigated.

III. RESULTS AND DISCUSSION

A. Broadband dielectric studies

The temperature dependence of the complex dielectric permittivity $\varepsilon^* = \varepsilon' - i\varepsilon''$ of all five investigated ceramics obtained at 1 kHz is shown in Fig. 1. Each composition shows just one maximum in $\varepsilon'(T)$ and $\varepsilon''(T)$ in the range of 275–325 K. The temperature dependences of the complex dielectric permittivity ε^* at various frequencies show typical relaxor behavior of all investigated ceramics, i.e., a shift of T_m with frequency. As an example, dielectric data of 0.4PZN-0.3PMN-0.3PSN ceramics are shown in Fig. 2.

For understanding the dielectric relaxation, it is more convenient to use a frequency plot of the complex permittivity at various representative temperatures—see Fig. 3. One can see a huge change of dielectric dispersion with temperature in 0.4PZN-0.3PMN-0.3PSN ceramics. At higher temperatures ($T \geqslant 400$ K), the dielectric loss dispersion is observed only at higher frequencies (more than 1 GHz). On cooling, the relaxation slows down and broadens. At temperatures around 300 K the relaxation becomes strongly asymmetric and very broad. On further cooling the dielectric dispersion becomes so broad that we can see only a part of it in our whole frequency range.

The symmetric dielectric dispersion at high temperatures can be easily described by the Cole-Cole formula

$$\varepsilon^*(\nu) = \varepsilon_{R\infty} + \frac{\Delta\varepsilon}{1 + (i\omega\tau_{CC})^{1-\alpha}}, \tag{1}$$

where $\Delta\varepsilon$ represents the dielectric strength of the relaxation, τ_{CC} is the mean Cole-Cole relaxation time, $\varepsilon_{R\infty}$ includes the contribution of all polar phonons and electronic polarization to the dielectric permittivity, and α is the Cole-Cole relaxation time distribution parameter; when $\alpha = 0$, Eq. (1) reduces to the Debye formula. The results of Cole-Cole fits are shown in Fig. 3 by solid lines. The temperature dependences

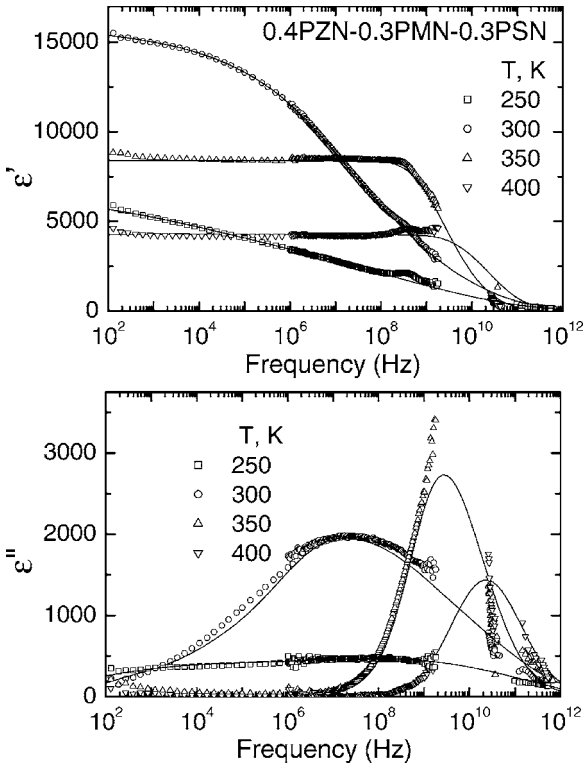

FIG. 3. Frequency dependence of the complex dielectric permittivity of 0.4PZN-0.3PMN-0.3PSN ceramics at several temperatures. Solid lines are the best fits with the obtained distribution of the relaxation times.

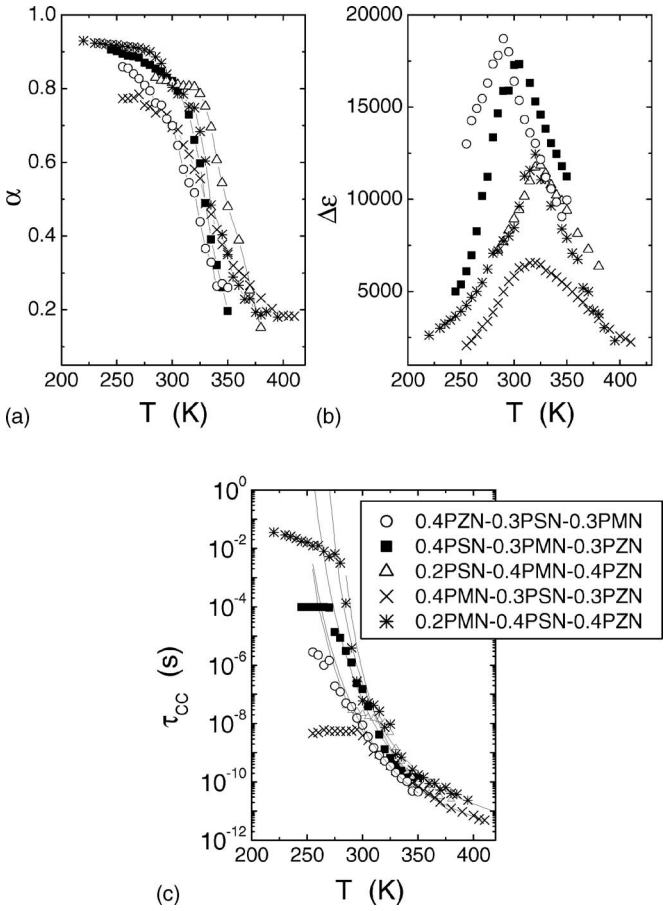

FIG. 4. Temperature dependence of the Cole-Cole parameters of the complex dielectric permittivity for the PZN-PMN-PSN ceramics. The $\tau_{CC}(T)$ lines in (c) were obtained from a Vogel-Fulcher fit.

of the Cole-Cole parameters obtained from the fits of all five investigated ceramics are presented in Fig. 4. One can see qualitatively the same behavior for all ceramics. The parameter α is small (<0.2) only at higher temperatures. On cooling this parameter increases, i.e., the distribution of relaxation times broadens. The mean Cole-Cole relaxation time τ_{CC} on cooling diverges according to the Vogel-Fulcher law

$$\tau_{CC} = \tau_0 \exp \frac{E}{k(T - T_0)}, \tag{2}$$

where T_0 is the Vogel-Fulcher or freezing temperature, and k denotes the Boltzmann constant. The obtained parameters are summarized in Table I. The maxima of the temperature dependences of $\Delta\varepsilon$ correspond to the maxima of the dielectric permittivity at lower frequencies, but the real temperature dependences of the static dielectric permittivity cannot be obtained below T_m, because the dielectric dispersion is too broad and part of it appears below our low-frequency limit. The Cole-Cole fit is not appropriate near T_m, because the absorption peak is not symmetric. Close to the freezing temperature the loss $\varepsilon''(\omega)$ does not exhibit any clear maximum so that the determination of the mean relaxation time τ_{CC} is not unambiguous. Therefore the Cole-Cole fit was not used below 220 or 250 K (depending on the composition). A more general approach has to be used for determination of the broad continuous distribution function of relaxation times $f(\tau)$ by solving the Fredholm integral equations[39]

$$\varepsilon(\omega)' = \varepsilon_{R\infty} + \Delta\varepsilon \int_{-\infty}^{\infty} \frac{f(\tau)d(\ln \tau)}{1 + \omega^2\tau^2}, \tag{3a}$$

$$\varepsilon''(\omega) = \Delta\varepsilon \int_{-\infty}^{\infty} \frac{\omega\tau f(\tau)d(\ln \tau)}{1 + \omega^2\tau^2}, \tag{3b}$$

with the normalization condition

$$\int_{-\infty}^{\infty} f(\tau)d(\ln \tau) = 1. \tag{4}$$

The solution of the integral equations (3) is known as the solution of an ill-posed problem. The most general method for the solution is Tikhonov regularization.[40–42] Application of this approach to relaxors was described in detail in Ref. 43.

The calculated distribution of relaxation times $f(\tau)$ for 0.4PZN-0.3PMN-0.3PSN ceramics is presented in Fig. 5. The temperature behavior of $f(\tau)$ was qualitatively the same in all investigated ceramics. A symmetric and narrow distribution of relaxation times is seen at higher temperatures. On cooling, the $f(\tau)$ function becomes asymmetrically shaped and a second maximum appears. The shortest and longest limits of the $f(\tau)$ function were calculated [level 0.1 of the

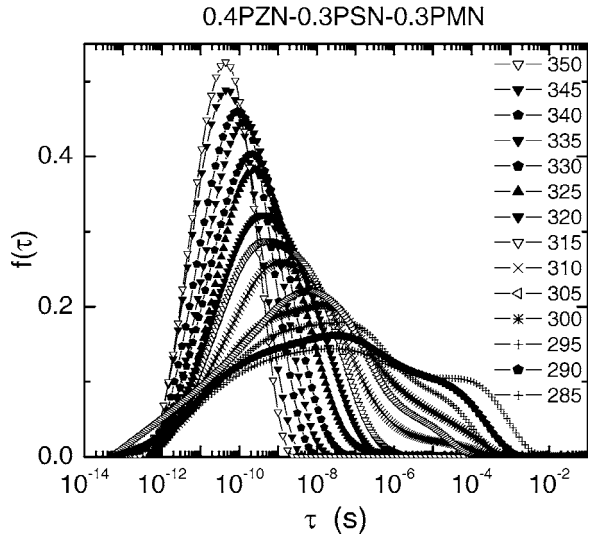

FIG. 5. Relaxation time distribution for 0.4PZN-0.3PMN-0.3PSN ceramics at various temperatures.

maximum $f(\tau)$ was chosen for definition of the limits] at various temperatures (Fig. 6). The shortest relaxation times τ_{min} have almost the same values 10^{-12}–10^{-13} s in all investigated ceramics and are temperature independent within the accuracy of our analysis. The longest relaxation times τ_{max} diverge according to the Vogel-Fulcher law (Fig. 6) and the obtained parameters are presented in Table II. The temperature dependences of both τ_{max} and τ_{min} are very similar to the results obtained for the relaxor PLZT ceramics.[20] The distribution function $f(\tau)$ was determined only at rather high temperatures, when the relaxation time lies within our experimental frequency range. Below T_m at 1 kHz τ_{max} appears much below our frequency limit, so we could not determine the static permittivity and therefore τ_{max} unambiguously.

The values of T_0 obtained from $\tau_{max}(T)$ in Table II are much higher than those from $\tau_{CC}(T)$ in Table I. Nevertheless, we clearly see that some dispersion remains below both freezing temperatures. One possible explanation is a distribution of Vogel-Fulcher temperatures T_0, where $0 \leqslant T_0 \leqslant T_0^{max}$.[44] In our case T_0^{max} would correspond to a Vogel-Fulcher temperature of $\tau_{max}(T)$. There is also another possible explanation of the anomalous broad dielectric dispersion of relaxors below the freezing temperature, if we assume that τ_{max} does not diverge near T_0, but has very large but finite values near and below T_0. The origin of the dielectric dispersion below the freezing temperature T_0 is rather nontrivial and will be discussed further below together with an explanation of the MW dielectric relaxation above T_m. Nevertheless, we see qualitatively similar behavior in all investigated samples: $f(\tau)$ has one maximum at high temperatures and it splits always near T_m into two parts. The first one follows the Vogel-Fulcher law, while the second one is only slightly temperature dependent and remains in the range of 10^{-8}–10^{-11} s. This is in contrast to dipolar glass systems, where only one $f(\tau)$ maximum was observed.[45]

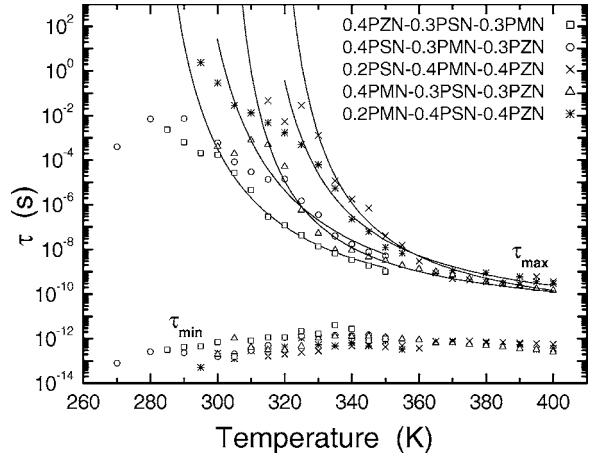

FIG. 6. Temperature dependences of the longest τ_{max} and shortest τ_{min} relaxation times in PZN-PMN-PSN ceramics. Solid lines are results of Vogel-Fulcher fit.

TABLE II. Parameters of the Vogel-Fulcher fit of the temperature dependences of the longest relaxation times τ_{max} in PZN-PMN-PSN ceramics.

Compound	τ_0 (s)	T_0 (K)	E/k (K)
0.4PZN-0.3PMN-0.3PSN	1.87×10^{-12}	272	518
0.4PSN-0.3PMN-0.3PZN	2.96×10^{-12}	303	425
0.2PSN-0.4PMN-0.4PZN	1.92×10^{-12}	311	384
0.4PMN-0.3PSN-0.3PZN	5.1×10^{-12}	297	333
0.2PMN-0.4PSN-0.4PZN	1×10^{-12}	280	668

B. THz dielectric spectra

The broadband dielectric spectra were obtained only up to 400 K; therefore Fig. 6 shows $f(\tau)$ only below this temperature. The answer to the question of how the relaxation behaves at higher temperatures can be given by THz dielectric spectroscopy, because the relaxation hardens in the MW and THz spectral range at high temperatures. Figure 7 shows the results of a time-domain THz transmission experiment obtained on 0.4PZN-0.3PMN-0.3PSN ceramics. The spectra of other PZN-PMN-PSN solid solutions exhibit qualitatively similar features: Above 80 K, the low-frequency THz permittivity ε' and losses ε'' rise, showing a dielectric relaxation contribution to the spectra. The relaxations do not contribute in the THz spectra below 80 K within our experimental errors; the dispersion in this THz range is determined only by phonon contributions. THz ε' and ε'' continuously increase on heating to 523 K due to the increase in the dielectric relaxation contribution as a consequence of increase in the mean relaxation frequency.

The relaxation stems from the dynamics of the polar clusters and it is well known that the polar clusters start to appear below the Burns temperature T_d.[8] Notice that THz ε' and ε'' values are highest at 523 K. This temperature is close to the Burns temperature in pure PMN. Nevertheless, one can see that the relaxation contributions gradually decrease on heating to 773 K and finally no dielectric relaxation is seen at 823 K (Fig. 7). The dielectric strength of the relaxation de-

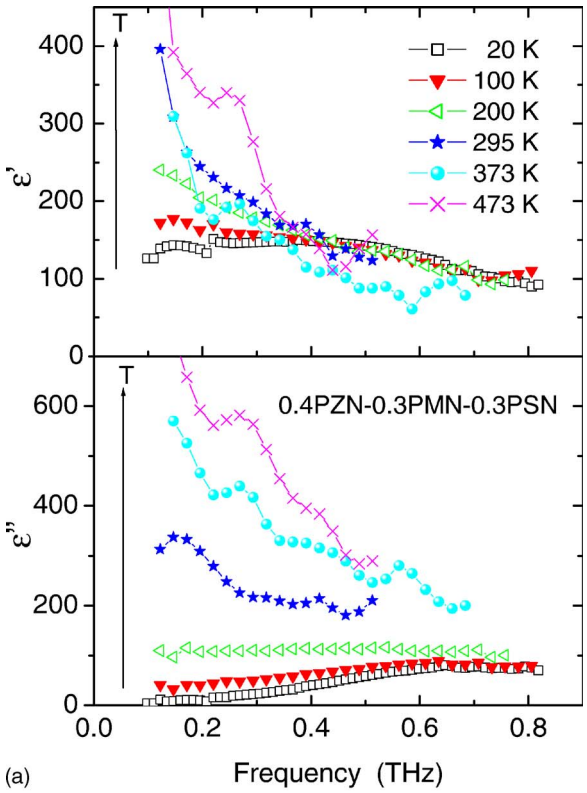

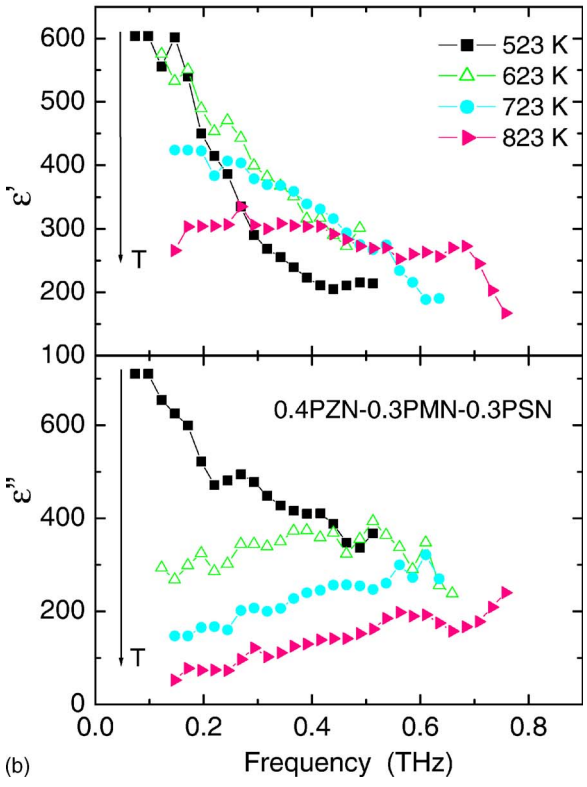

FIG. 7. (Color online) Complex THz dielectric spectra of 0.4PZN-0.3PMN-0.3PSN ceramics (a) below 473 K and (b) above 523 K. The arrow near T marks the direction of temperature rise.

creases on heating above 523 K as a consequence of decrease in the polar cluster concentration. It would mean that some polar clusters persist at least up to 773 K, i.e., the Burns temperature lies higher than in pure PMN. Note that similar behavior, i.e., an unusual decrease in dielectric losses on heating above T_d, was also observed in a PMN thin film ≈670 K.[16] This phenomenon was also explained by disappearance of the relaxation (central mode) and soft mode hardening above T_d (see the discussion below).[16]

Let us discuss the origin and temperature dependence of the distribution function $f(\tau)$ (Fig. 5) together with the THz spectra. One symmetric and relatively narrow maximum is seen above 320 K in the THz and MW range. The dielectric relaxation is caused predominantly by flipping, but also partially by breathing (i.e., fluctuations of the cluster volume) of polar clusters at high temperatures. At lower temperatures the $f(\tau)$ function broadens and splits into two parts. The part at higher τ (mainly due to cluster flipping) anomalously slows down according to the Vogel-Fulcher law (see Fig. 6) and disappears below the freezing temperature T_0. The higher-frequency part describes mainly breathing of the polar clusters. The breathing is a temperature-activated process; therefore it slows down on cooling according to the Arrhenius law. Large chemical disorder at the B perovskite sites causes random fields on disordered Pb atoms, which are most likely responsible for the anomalous broadening of $f(\tau)$ on cooling. Finally, $f(\tau)$ becomes almost flat between τ_{min} and τ_{max}. Below T_0, the τ_{max} shifts many orders of magnitude below our frequency range; therefore it was not evaluated from our spectra. Nevertheless, due to the expected increase of τ_{max} on cooling and due to the normalization condition Eq. (4), one can expect decrease of both ε' and ε'' at low temperatures. The THz dielectric spectra show influence of the dielectric relaxation down to 80 K. This means that τ_{min} remains almost constant in the THz region down to very low temperatures. In other words, it means that there is a continuous distribution of activation energies for anharmonic hopping of Pb atoms from some maximum energy E_{max} essentially to 0. The energy E_{max} could be in principle obtained from the Arrhenius law

$$\tau_{max} = \tau_0 \exp \frac{E_{max}}{kT} \tag{5}$$

fit of $\tau_{max}(T)$ below T_0; however, such a fit was not possible due to the lack of very-low-frequency dielectric data. From the same reason $f(\tau)$ in Fig. 5 was determined only above T_0.

The nature of the polar nanoclusters and two-component dielectric relaxation is still under debate. Very recently Blinc *et al.*[45] suggested that ^{207}Pb NMR spectra give evidence for the two-component nature of relaxors—a glassy matrix (corresponding to spherical displacements of Pb ions) and frozen polar nanoclusters (due to the Pb displacements in the [111] directions). These two components could be responsible, according to Blinc *et al.*, also for the two-component dielectric relaxation.[45] Xu *et al.*[46] published recently some evidence that the polar clusters have polarizations along the [110] directions, and that these clusters persist even in poled ferroelectric PZN with polarization along the [111] directions. Our opinion[15] is that the two dielectric relaxation regions have origin in the flipping and breathing of the polar clusters, but the subject needs still further investigation.

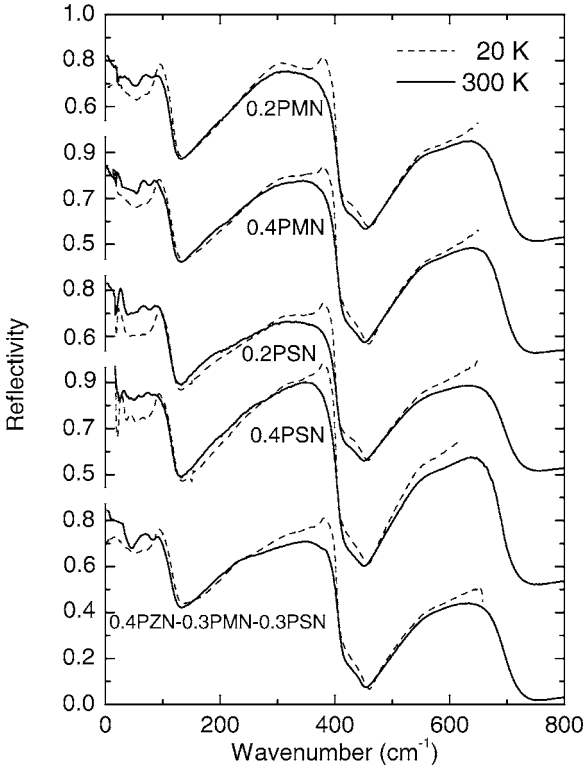

FIG. 8. Infrared reflectivity spectra of the investigated ceramic systems at 20 and 300 K. Assignment of the samples is shortened; only the first part of the composition is marked. The full composition of the samples is listed in Table I.

C. Infrared reflectivity studies

Experimental IR reflectivity spectra of all five investigated ceramics, taken at 20 and 300 K, are shown in Fig. 8. One can see that the spectra are similar, i.e., the frequencies and strengths of all phonon modes are very similar to each other in all samples. The spectral range above 800 cm^{-1} is not shown because the reflectivity is almost flat in this frequency region.

Infrared and THz reflectivity spectra of 0.4PZN-0.3PMN-0.3PSN ceramics taken at various temperatures are shown in Fig. 9. THz reflectivity at the low-frequency end was calculated from the THz transmission spectra. Infrared and THz spectra were fitted simultaneously using a generalized-oscillator model with the factorized form of the complex permittivity:

$$\varepsilon^*(\omega) = \varepsilon_\infty \prod_j \frac{\omega_{LOj}^2 - \omega^2 + i\omega\gamma_{LOj}}{\omega_{TOj}^2 - \omega^2 + i\omega\gamma_{TOj}} \tag{6}$$

where ω_{TOj} and ω_{LOj} mark the transverse and longitudinal frequencies of the jth mode, respectively, and γ_{TOj} and γ_{LOj} denote their corresponding damping constants. $\varepsilon^*(\omega)$ is related to the reflectivity $R(\omega)$ by

$$R(\omega) = \left| \frac{\sqrt{\varepsilon^*(\omega)} - 1}{\sqrt{\varepsilon^*(\omega)} + 1} \right|^2. \tag{7}$$

The high-frequency permittivity ε_∞ resulting from the electronic absorption processes was obtained from the frequency-independent room-temperature reflectivity above the phonon frequencies. The temperature dependence of ε_∞ is usually very small and was neglected in our fits. Eight polar phonons were resolved in the IR spectra below 150 K; seven modes at higher temperatures. Similar behavior was observed in other PZN-PMN-PSN ceramics. It is inconsistent with the factor-group analysis for the cubic and rhombohedral symmetry, where three and 16 active modes, respectively, are allowed in the IR spectra. The coherence length for the IR activity is quite short (determined by the range of interatomic forces), which could enable us to see the local polar distortions in polar clusters, i.e., polar modes from the rhombohedral structure could be seen in our IR spectra. We do not see all of them because some of them could be weak and/or overlapped with others due to their finite widths.

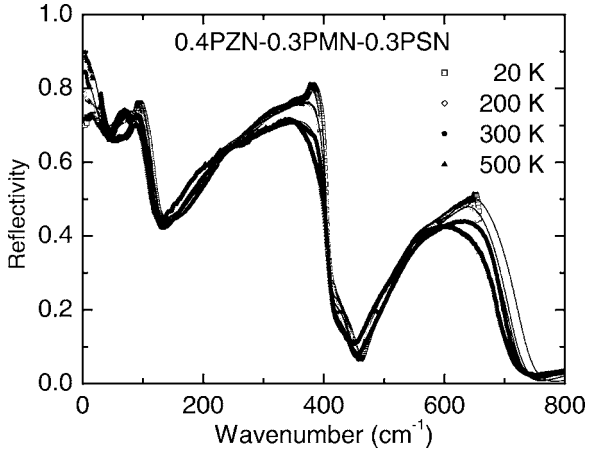

FIG. 9. Infrared and THz reflectivity spectra of 0.4PZN-0.3PMN-0.3PSN ceramics at various temperatures. Solid lines are results of the fits.

The real and imaginary parts of $\varepsilon^*(\omega)$ obtained from the fits of IR reflectivity and THz dielectric spectra in Fig. 9 are shown in Fig. 10. The low-frequency part of the IR and THz spectra was fitted with an overdamped oscillator. This model cannot completely fit the MW relaxation and the static permittivity (see Sec. III A), but it can roughly describe the high-frequency wing of the MW relaxation seen in the THz spectra. On heating, the dielectric contribution of this overdamped oscillator increases with temperature (up to 500 K) and its relaxation frequency (maximum of losses) hardens and approaches the THz range.

Interesting phonon anomalies were observed in all the investigated ceramics. Most phonon frequencies show some softening on heating, but the most remarkable softening is displayed by the lowest-frequency TO_1 phonon. A similar soft TO_1 mode was observed in pure PMN and PST. This mode was explained as a ferroelectric soft mode within polar clusters, which shows a tendency to soften toward the Burns temperature.[15,16,19] Its frequency follows the Cochran law

$$\omega_{SM}^2 = A(T_{cr} - T) \tag{8}$$

where A is a constant and T_{cr} means the critical softening temperature and appears close to T_d. The obtained param-

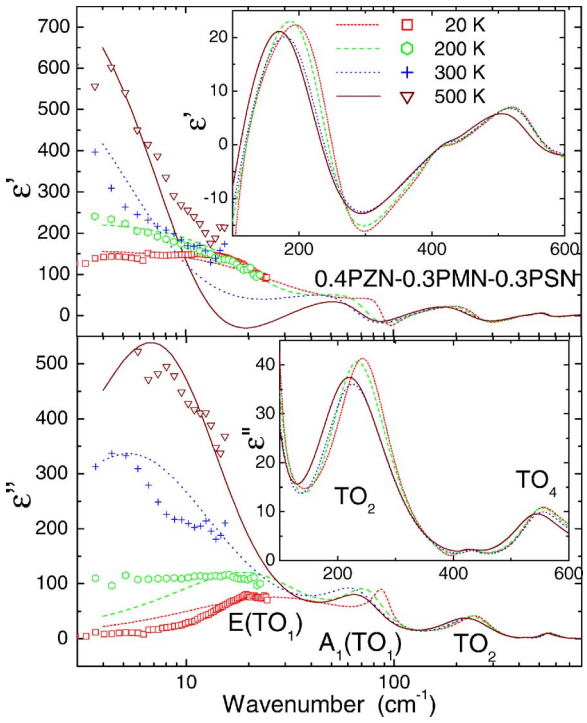

FIG. 10. (Color online) Complex dielectric permittivity obtained from the fit of IR and THz spectra of 0.4PZN-0.3PMN-0.3PSN ceramics. The points are experimental THz data.

eters of the fits according to Eq. (8) are listed in Tables III and IV. T_{cr1} of the TO_1 mode fluctuates between 600 and 860 K, and it is difficult to speculate that these temperatures correspond to Burns temperatures, because the softening has ceased already above 350 or 400 K. Nevertheless, it is worth noting that in 0.4PZN-0.3PMN-0.3PSN ceramics the dielectric relaxation (the polar clusters) vanishes above 773 K, which is comparable to T_{cr}=747 K for the TO_1 mode.

Noncomplete softening of TO_1 mode was observed in all previously studied RFEs.[50] For example, in pure PMN,[16] the soft mode follows the Cochran law up to 450 K but levels off at higher temperatures. Recently, Toulouse *et al.*[47] investigated PZN relaxor by means of Raman scattering and reported a new characteristic temperature near 470 K, which he called the temperature of the local phase transition or the temperature of polar cluster formation. According to Toulouse *et al.* the Burns temperature is the temperature below which the anharmonic vibrations of Pb atoms become slower than the frequency of the F_{1u} soft phonon mode. Dkhil

TABLE III. Parameters of the Cochran fit to TO_1 modes in PZN-PMN-PSN ceramics.

Compound	A (cm^2/K)	T_{cr1} (K)
0.4PZN-0.3PMN-0.3PSN	9.82	830
0.4PSN-0.3PMN-0.3PZN	12.66	599
0.2PSN-0.4PMN-0.4PZN	11.1	820
0.4PMN-0.3PSN-0.3PZN	13.22	636
0.2PMN-0.4PSN-0.4PZN	10.05	849

TABLE IV. The parameters of Cochran's fit of TO_2 modes in PZN-PMN-PSN ceramics.

Compound	A (cm^2/K)	T_{cr2} (K)
0.4PZN-0.3PMN-0.3PSN	40.15	1641
0.4PSN-0.3PMN-0.3PZN	26.15	1975
0.2PSN-0.4PMN-0.4PZN	45.97	1231
0.4PMN-0.3PSN-0.3PZN	44.01	1526
0.2PMN-0.4PSN-0.4PZN	37.76	1922

et al.[48] reported also a new temperature T_l located between the Burns T_d and freezing T_f temperature. They observed an increase of the diffuse scattering in PMN below $T_l \approx 400$ K as well as a plateau in the temperature-dependent lattice constant between T_l and T_f. Unfortunately, we could not study the IR reflectivity spectra above 500 K due to the limitation of our furnace. For the investigation of $TO_1(T)$ above T_d, far-IR transmission spectroscopy of thin films deposited on a transparent substrate like sapphire or MgO is more suitable.[16] We speculate that the T_l temperature corresponds to the temperature below which the polar clusters percolate; namely, in the system of nonpercolated polar clusters the effective soft-mode frequency cannot completely soften,[49] being increased by the depolarization field at the boundary between the clusters and the nonpolar matrix. Therefore the leveling off (or even increase) of the soft-mode frequency seen above $T_l \approx 400$ K could be the result of breaking of the percolated polar clusters.

Surprisingly, the TO_2 mode frequency also partially softens on heating following the Cochran dependence [see Fig. 11(b)]. This mode describes predominantly vibration of the B atoms against the oxygen octahedra.[50] The B sites exhibit large chemical disorder (four different ions of different valency) and the T_{cr2} temperature may correspond to the temperature above which the B-site atoms can diffuse (higher than the sintering temperature of 1000 K).

The list of polar mode parameters in 0.4PZN-0.3PMN-0.3PSN ceramics is summarized in Table V. The parameters of the other investigated ceramics are very similar and comparison with pure PMN (Refs. 50 and 51) as well as with PS (Ref. 52) or with PMN-PT (Refs. 50 and 53) shows that the spectra of all perovskite RFEs have the same features: The three F_{1u} cubic perovskite modes are split due to a lower symmetry in the polar (or chemical) nanoclusters. The most remarkable splitting is seen in the soft mode at low temperatures. Its A_1 component has frequency near 90 cm^{-1}, while the E component is heavily damped with frequency near 20 cm^{-1}. Detailed assignment of the polar modes in perovskite RFEs was recently thoroughly discussed:[50] The modes below 100 cm^{-1} in Pb-containing RFEs correspond predominantly to the vibration of rigid BO_6 octahedra against Pb atoms (the so-called Last mode). The two modes between 200 and 300 cm^{-1} are A_1 and E components corresponding to the vibration of the B atoms against the O_6 octahedra (so called Slater mode) and the modes above 500 cm^{-1} correspond to bending of the O_6 octahedra (the so called Axe mode). The mode near 350 cm^{-1} is activated in the spectra probably due to the local order in the B sites which would

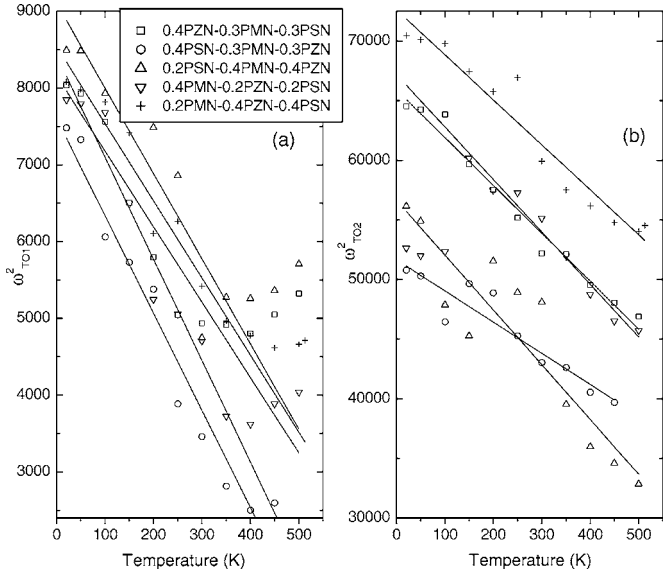

FIG. 11. Cochran fits to (a) TO_1 and (b) TO_2 modes in PZN-PMN-PSN solid solutions.

correspond to mutual *B*-atom vibrations. Hlinka *et al.*[54] recently used the effective medium approximation for the evaluation of room-temperature IR reflectivity spectra of PMN and showed that this approach can be used for determination of the anisotropic dielectric function of the polar clusters. From this analysis it follows that the mode near 400 cm^{-1} (seen also in our spectra) is not a real polar phonon, but just an apparent mode which appears in the IR spectra as a consequence of geometrical resonances between the two longitudinal mode frequencies.[54]

Figure 10 shows a broad maximum of $\varepsilon''(\omega)$ near 30 cm^{-1} which should correspond to the *E* component of the soft mode. This mode softens to $\approx$20 cm^{-1} at 200 K; however, at higher temperatures it becomes overlapped by the dielectric relaxation which approaches this frequency range (the loss peak below 10 cm^{-1}). Above the Burns temperature, the *E* mode should merge with the A_1 mode where only triply degenerate F_{1u} modes are expected and the dielectric relaxation due to the polar clusters should vanish.

IV. CONCLUSIONS

Concluding, a broadband dielectric investigation of several PZN-PMN-PSN ceramics revealed qualitatively similar behavior, which seems to appear similarly for all perovskite RFEs. In IR spectra additional polar phonon modes are activated (forbidden in the cubic structure) due to the broken cubic symmetry in polar clusters. The TO_2 polar mode softens according to the Cochran law; this effect was not observed in other relaxor ferroelectrics. The A_1 component of the ferroelectric TO_1 soft mode in polar clusters follows the Cochran law below 400 K. Above 400 K, it levels off, because the polar clusters cease percolating above this temperature. The *E* component of the soft mode is heavily damped at a frequency near 20 cm^{-1}. It is overlapped with the dielectric relaxation in the THz range which stems from flipping of polar clusters. The THz relaxation appears gradually on cooling below 800 K, giving evidence of a smeared Burns temperature. The relaxation slows down on cooling and splits into two parts. The lower-frequency part anomalously broadens and follows the Vogel-Fulcher law above the freezing temperature. The higher-frequency component of the relaxation softens much slower. We suggested an explanation of the two-component relaxation, but further studies are needed to confirm it.

TABLE V. Polar mode parameters of the 0.4PZN-0.3PMN-0.3PSN ceramics obtained from the fit to the 20 K reflectivity. All parameters are in cm^{-1}; ε_∞=5.4.

ω_{TO}	γ_{TO}	ω_{LO}	γ_{LO}
17.5	17.5	23.2	56.9
91.7	29.5	119.1	27.4
266.6	170.4	404.7	19.2
296.2	340.6	294.2	441.9
358.3	112.8	352	88.1
405.7	62.1	447.9	37.9
533.2	105.5	735.4	41.9
623.9	100.6	615.7	137

ACKNOWLEDGMENTS

We would like to thank D. Noujni for the technical help with the IR experiment. The work has been supported by the Grant Agency of the Czech Republic (Projects No. 202/06/0403 and No. 202/04/0993), and the Lithuanian Science and Study Foundation.

*Electronic address: jan.macutkevic@ff.vu.lt

[1] R. Pirc and R. Blinc, Phys. Rev. B **60**, 13470 (1999).
[2] G. A. Samara, in *Solid State Physics, Advances in Research and Applications* (Academic Press, San Diego, 2001), Vol. 56, pp. 240–458, and references therein.
[3] N. de Mathan, E. Husson, G. Calvarin, J. R. Gavarri, A. W. Hewat, and A. Morell, J. Phys.: Condens. Matter **3**, 8159 (1991).
[4] C. Malibert, B. Dkhil, J. M. Kiat, D. Durand, J. F. Bérar, A. Spasojevic-de Biré, J. Phys.: Condens. Matter **9**, 7485 (1997).
[5] C. Perrin, N. Menguy, E. Suard, Ch. Muller, C. Caranoni, and A. Stepanov, J. Phys.: Condens. Matter **12**, 7523 (2000).
[6] G. A. Smolenskii, V. A. Isupov, A. I. Agranovskaya, and S. N. Popov, Sov. Phys. Solid State **2**, 2584 (1961).
[7] Y. Yokomizo, T. Takahashi, and Y. Yamashita, Jpn. J. Appl. Phys., Part 1 **37**, 3382 (1998).
[8] G. Burns and F. H. Dacol, Solid State Commun. **48**, 853 (1983); Phys. Rev. B **28**, 2527 (1983).

[9] K. Hirota, Z.-G. Ye, S. Wakimoto, P. M. Gehring, and G. Shirane, Phys. Rev. B **65**, 104105 (2002).
[10] I.-K. Jeong, T. W. Darling, J. K. Lee, Th. Proffen, R. H. Heffner, J. S. Park, K. S. Hong, W. Dmowski, and T. Egami, Phys. Rev. Lett. **94**, 147602 (2005).
[11] S. Vakhrushev, S. Zhukov, G. Fetisov, and V. Chernyshov, J. Phys.: Condens. Matter **6**, 4021 (1994).
[12] P. K. Davies and M. A. Akbas, J. Phys. Chem. Solids **61**, 159 (2000).
[13] Y. L. Wang, S. S. N. Bharadwaja, A. K. Tagantsev, and N. Setter, J. Eur. Ceram. Soc. **25**, 2521 (2005).
[14] B. P. Burton, E. Cockayne, and U. V. Waghmare, Phys. Rev. B **72**, 064113 (2005).
[15] V. Bovtun, S. Kamba, A. Pashkin, M. Savinov, P. Samoukhina, and J. Petzelt, Ferroelectrics **298**, 23 (2004).
[16] S. Kamba, M. Kempa, V. Bovtun, J. Petzelt, K. Brinkman, and N. Setter, J. Phys.: Condens. Matter **17**, 3965 (2005).
[17] F. Chu, N. Setter, C. Elissalde, and J. Ravez, Mater. Sci. Eng., B **38**, 171 (1996).
[18] V. Bovtun, V. Porokhonskyy, J. Petzelt, M. Savinov, J. Endal, C. Elissalde, and C. Malibert, Ferroelectrics **238**, 17 (2000).
[19] S. Kamba, M. Berta, M. Kempa, J. Hlinka, J. Petzelt, K. Brinkman, and N. Setter, J. Appl. Phys. **98**, 074103 (2005).
[20] S. Kamba, V. Bovtun, J. Petzelt, I. Rychetsky, R. Mizaras, A. Brilingas, J. Banys, and M. Kosec, J. Phys.: Condens. Matter **12**, 497 (2000).
[21] I. Rychetsky, S. Kamba, V. Porokhonskyy, A. Pashkin, M. Savinov, V. Bovtun, J. Petzelt, M. Kosec, and M. Dressel, J. Phys.: Condens. Matter **15**, 6017 (2003).
[22] S.-E. Park and T. S. Shrout, J. Appl. Phys. **92**, 1804 (1997).
[23] B. Noheda, Curr. Opin. Solid State Mater. Sci. **6**, 27 (2002).
[24] N. Fu and R. E. Cohen, Nature (London) **403**, 281 (2000), and references therein.
[25] M. Dambekalne, I. Brante, M. Antonova, and A. Sternberg, Ferroelectrics **131**, 67 (1992).
[26] L. Farber, M. Valant, M. A. Akbas, and P. K. Davies, J. Am. Ceram. Soc. **85**, 2319 (2002).
[27] L. Farber and P. Davies, J. Am. Ceram. Soc. **86**, 1961 (2003).
[28] I. P. Raevski, S. M. Emelyanov, F. I. Savenko, I. N. Zakharchenko, O. A. Bunina, M. A. Malitskaya, A. S. Bogatin, and E. V. Sahkar, Ferroelectrics **285**, 283 (2003).
[29] I. P. Raevski, S. A. Prosandeev, S. M. Emelyanov, F. I. Savenko, I. N. Zakharchenko, O. A. Bunina, A. S. Bogatin, S. I. Raevskaja, E. S. Gagarina, E. V. Sahkar, and L. Jastrabik, Integr. Ferroelectr. **53**, 475 (2003).
[30] D. H. Zhou, G. L. Hoatson, R. L. Vold, and F. Fayon, Phys. Rev. B **69**, 134104 (2004).
[31] K. Bormanis, A. I. Burkhanov, A. V. Alpatov, M. Dambekalne, A. Kalvane, A. Sternberg, and A. V. Shil'nikov, Ferroelectrics **318**, 209 (2005).
[32] M. Dambekalne, K. Bormanis, A. Sternberg, and I. Brante, Ferroelectrics **240**, 221 (2000).
[33] J. Macutkevic, S. Lapinskas, J. Grigas, A. Brilingas, J. Banys, R. Grigalaitis, K. Meskonis, K. Bormanis, A. Sternberg, and V. Zauls, J. Eur. Ceram. Soc. **25**, 2415 (2005).
[34] J. Banys, J. Macutkevic, A. Brilingas, J. Grigas, K. Bormanis, and A. Sternberg, Ferroelectrics **318**, 141 (2005).
[35] J. L. Dellis, I. P. Raevski, S. I. Raevskaja, and L. A. Reznitchenko, Ferroelectrics **318**, 169 (2005).
[36] S. A. Seo, K. H. Noh, and S. I. Kwun, J. Korean Phys. Soc. **35**, 496 (1999).
[37] W. Kleemann and R. Lindner, Ferroelectrics **199**, 1 (1997).
[38] J. Grigas, *Microwave Dielectric Spectroscopy of Ferroelectric and Related Materials* (Gordon and Breach Science Publishers, Amsterdam, 1996).
[39] H. Schäfer, E. Sternin, R. Stannarius, M. Arndt, and F. Kremer, Phys. Rev. Lett. **76**, 2177 (1996).
[40] A. N. Tikhonov and V. Y. Arsenin, *Solution of Ill-Posed Problems* (Wiley, New York, 1977).
[41] C. W. Groetsch, *The Theory of Tikhonov regularization for Fredholm Equation* (Pitman, London, 1984).
[42] S. W. Provencher, Comput. Phys. Commun. **27**, 213 (1982).
[43] J. Macutkevic, J. Banys, and A. Matulis, Nonlin. Anal. Model. Control **9**, 1 (2004).
[44] R. Pirc, R. Blinc, and V. Bobnar, Phys. Rev. B **63**, 054203 (2001).
[45] R. Blinc, V. V. Laguta, B. Zalar, and J. Banys, J. Mater. Sci. **41**, 27 (2006).
[46] Guangyong Xu, Z. Zhong, Y. Bing, Z.-G. Ye, and G. Shirane, Nat. Mater. **5**, 134 (2006).
[47] J. Toulouse, F. Jiang, O. Svitelskiy, W. Chen, and Z.-G. Ye, Phys. Rev. B **72**, 184106 (2005).
[48] B. Dkhil, J. M. Kiat, G. Calvarin, G. Baldinozzi, S. B. Vakhrushev, and E. Suard, Phys. Rev. B **65**, 024104 (2002).
[49] I. Rychetský and J. Petzelt, Ferroelectrics **303**, 137 (2004).
[50] J. Hlinka, J. Petzelt, S. Kamba, D. Noujni, and T. Ostapchuk, Phase Transitions **79**, 41 (2006).
[51] S. A. Prosandeev, E. Cockayne, B. P. Burton, S. Kamba, J. Petzelt, Yu. Yuzyuk, R. S. Katiyar, and S. B. Vakhrushev, Phys. Rev. B **70**, 134110 (2004).
[52] J. Petzelt, E. Buixaderas, and A. V. Pronin, Mater. Sci. Eng., B **55**, 86 (1998).
[53] S. Kamba, E. Buixaderas, J. Petzelt, J. Fousek, J. Nosek, and P. Bridenbaugh, J. Appl. Phys. **93**, 933 (2003).
[54] J. Hlinka, T. Ostapchuk, D. Noujni, S. Kamba, and J. Petzelt, Phys. Rev. Lett. **96**, 027601 (2006).